



THE UNIVERSITY *of* EDINBURGH

Edinburgh Research Explorer

Methodology for Estimating Pyrolysis Rates of Charring Insulation Materials using Experimental Temperature Measurements

Citation for published version:

Hidalgo-Medina, J, Gerasimov, N, Hadden, R, Torero, JL & Welch, S 2016, 'Methodology for Estimating Pyrolysis Rates of Charring Insulation Materials using Experimental Temperature Measurements', *Journal of Building Engineering*, vol. 8, pp. 249-259. <https://doi.org/10.1016/j.jobe.2016.09.007>

Digital Object Identifier (DOI):

[10.1016/j.jobe.2016.09.007](https://doi.org/10.1016/j.jobe.2016.09.007)

Link:

[Link to publication record in Edinburgh Research Explorer](#)

Document Version:

Peer reviewed version

Published In:

Journal of Building Engineering

General rights

Copyright for the publications made accessible via the Edinburgh Research Explorer is retained by the author(s) and / or other copyright owners and it is a condition of accessing these publications that users recognise and abide by the legal requirements associated with these rights.

Take down policy

The University of Edinburgh has made every reasonable effort to ensure that Edinburgh Research Explorer content complies with UK legislation. If you believe that the public display of this file breaches copyright please contact openaccess@ed.ac.uk providing details, and we will remove access to the work immediately and investigate your claim.



1 Methodology for Estimating Pyrolysis Rates of Charring Insulation Materials 2 using Experimental Temperature Measurements

3 Juan Patricio Hidalgo^{a1,2}, Nikolai Gerasimov^a, Rory Miles Hadden^a, José Luis Torero^b, and Stephen
4 Welch^a

5 ^a School of Engineering, The University of Edinburgh, Edinburgh, EH9 3JL, UK

6 ^b School of Civil Engineering, The University of Queensland, Brisbane St Lucia, QLD 4072, Australia

7 Abstract

8 This paper presents the application of a simplified method to estimate pyrolysis rates from rigid closed-cell
9 cellular plastics by means of experimental temperature measurements. These materials are extremely
10 effective in meeting energy efficiency goals in buildings and their safe use should also be enabled and
11 optimised by undertaking comprehensive fire safety analyses. The proposed methodology consists of
12 determining the mass loss as a function of the thermal evolution by applying a mass conversion directly
13 using thermogravimetric data under non-oxidative conditions. In order to verify this simplified method, an
14 experimental programme based on 100 mm thick samples of rigid polyisocyanurate foam was conducted
15 using a Cone Calorimeter, obtaining measurements of mass loss and temperature within the core of the
16 material. A Monel plate was used on top of the sample in order to represent a simpler boundary condition
17 by eliminating the smouldering process of the charred material. Although the pyrolysis rates using this
18 methodology did not provide a perfect fit with experimental data, they showed similar trends, with a slightly
19 delayed prediction but still accurate magnitude. This methodology presents potential for fire safety
20 engineering applications in two domains: (1) as a complementary technique to improve the interpretation
21 of results from standard and ad-hoc testing, and (2) as a design technique for the evaluation of potential
22 heat release contribution and gaseous emissions of assemblies incorporating insulation materials.

23 Keywords

24 Insulation materials; Fire Safety; Pyrolysis; Modelling; Performance-based design; Charring

¹ Corresponding author: j.hidalgo@uq.edu.au

² Present address: School of Civil Engineering, The University of Queensland, Brisbane St Lucia, QLD 4072, Australia

25 Nomenclature

k	thermal conductivity ($\text{W}\cdot\text{m}^{-1}\cdot\text{K}^{-1}$)
c	specific heat capacity ($\text{J}\cdot\text{kg}^{-1}\cdot\text{K}^{-1}$)
f	non-dimensional fraction of remaining mass (-)
i	number of element (-)
j	number of time step (-)
k	number of exposure area (-)
L	thickness (m)
m	mass (g)
\dot{m}	mass flow ($\text{g}\cdot\text{s}^{-1}$)
\dot{m}''	mass loss rate per unit area ($\text{g}\cdot\text{s}^{-1}\cdot\text{m}^{-2}$)
N	maximum number of finite differences (-)
q	heat (W)
t	time (s)
S	surface area (m^2)
T	temperature (K or °C)
x	distance (m)
Y	yield ($\text{g}\cdot\text{g}^{-1}$)

Greek letters

α	absorptivity/emissivity (-)
ΔH_c	effective heat of combustion ($\text{J}\cdot\text{kg}^{-1}\cdot\text{K}^{-1}$)
Δt	time step (s)
Δx	finite difference thickness (m)
ρ	density ($\text{kg}\cdot\text{m}^{-3}$)

Subscripts

0	initial
cr	critical
i	of the difference i
net	net/conductive
P	pyrolysis
z	species

Acronyms

HRR	heat release rate
MLR	mass loss rate
PIR	rigid closed-cell polyisocyanurate foam
SIP	structural insulated panel

TC	thermocouple
TGA	thermogravimetric analysis
U-value	thermal transmittance

26 **1. Introduction**

27 During recent decades sustainability has become one of the main drivers in building construction,
28 resulting in highly thermally efficient buildings. Several techniques may be used to achieve the stringent
29 energy efficiency requirements defined by the Energy Performance of Buildings Directive [1], e.g. thermal
30 insulation within the building envelope, increased levels of air tightness, efficient heat recovery of the
31 ventilation systems, reduction of thermal bridging and/or more efficient windows [2]. The intense use of
32 thermal insulation is one of the primary targets due to the large surface area of the building envelope and
33 the architectural aspirations. As a result, low thermal transmittances (*U-values*) are required, which can
34 only be achieved by significantly increasing the thickness of insulation used.

35 Due to the multi-criteria nature of building design, stringent *U-values* clash with other desired design
36 criteria such as efficient space usage and cost. Despite the large diversity of insulation materials in the
37 market [3], under this competitive scenario closed-cell plastic foams have become an easy and cost-
38 effective solution because of their relatively low thermal conductivity. The most common closed-cell
39 insulation foams at present being used are rigid polyisocyanurate foams, commonly known as PIR, and
40 phenolic foam. These materials are often provided as boards with a foil-facing on the surface and used for
41 framing construction or masonry cavity walls; alternatively they can be embedded directly within linings,
42 e.g. sandwich panels or structural insulated panels (SIPs) [4].

43 Despite the fact that these materials are extremely effective in meeting energy efficiency goals, their use
44 should be also enabled and optimised by undertaking a comprehensive fire safety analysis, i.e. systems
45 including insulation materials should be optimised while still ensuring life safety and property protection.

46 **1.1. Fire performance of closed-cell plastic insulation materials**

47 The fire performance of these materials has been studied by several authors at different scales [5–19].
48 Generally, these types of plastics are classified either as thermoplastics or thermosets. Thermoplastics (e.g.
49 expanded polystyrene) exhibit melting behaviour, while thermosets (e.g. polyisocyanurate or phenolic
50 foam) exhibit a charring behaviour, leaving a carbonaceous residue after pyrolysis. A complete description
51 of the different mechanisms of thermal decomposition for these polymers is described by *Witkowski et al.*
52 [5]. These mechanisms result in different fire performance, with a charring behaviour being more desirable
53 due to the positive effect of the char layer on the reduction of the pyrolysis rate. Several authors have
54 focussed their research at the material scale (e.g. thermogravimetry), looking at polymer formulations that

55 promote larger residue generation and endothermic reactions in the solid-phase [6–8]. These techniques of
56 flame retardancy have been largely covered by *Hull and Kandola* [9]. However, the majority of research
57 has focussed on the macroscopic material behaviour using bench-scale testing, thus concentrating on the
58 ignition mechanism and release of heat from these materials [10–19]. More extensive experimental work
59 covering different scales can be found in references **Error! Reference source not found.** and **Error!
60 Reference source not found.**

61 Recently published work showed the relation between the thermal degradation at the material scale
62 linked to the heat transfer phenomena within the solid material [20]. Rigid closed-cell polyisocyanurate and
63 phenolic foam showed similar behaviour, i.e. materials that experience pyrolysis and char formation. The
64 char layer reduces the heat transport to the pyrolysis front resulting in a slower propagation and lower
65 pyrolysis rate. Typically, this insulating effect of the surface char layer limits the heating of virgin foam to
66 several degrees per minute. Experimental results showed that this char is however highly vulnerable to
67 surface oxidation (smouldering). The smouldering process was shown not to be self-sustaining due to the
68 large heat losses under the specific experimental conditions. In addition, the closed-cell structure of the
69 polymer restricted the air flow through the foam which was shown to be a key factor to limit self-sustaining
70 smouldering [20]. In end-use conditions, the insulation materials are typically covered by a lining or a
71 physical barrier, thus limiting the contact with the air, unless they are introduced in partial fill cavity walls.
72 As a result, this smouldering behaviour is not expected under real fire conditions. Therefore, initially only
73 pyrolysis should be considered as the primary hazardous event.

74 **1.2. Fire safe design of insulation materials**

75 It has been widely recognised that the organic polymer nature of closed-cell plastic foams may represent
76 a fire risk in buildings [21–23]. The fire safe design of building assemblies including insulation materials
77 has been classically based on a material classification and a pass-fail criteria frameworks, e.g. in the EU
78 represented by the Euroclasses system [24] and the fire-resistance framework [25], respectively. The
79 prescriptive nature of these frameworks however does not allow for a quantitative design to be carried out
80 on the basis of the specific insulation fire hazards, and as a result it is not possible to quantify the associated
81 fire risk [26].

82 Previous work demonstrated that the initiating hazard from this type of insulation material corresponds
83 to the onset of pyrolysis [26]. After this is achieved, there is potential for the generation of a large amount
84 of flammable gases that may be transported to the compartment fire, or alternatively may escape to areas
85 away from the fire enclosure. The former may represent an increase in the heat release rate of the fire, while
86 the latter may represent a life safety hazard for the occupants of the building due to the intrinsic toxicity of

87 the pyrolysis effluent. Current mitigation practices are thus based on the design of suitable thermal barriers
88 that delay or cancel the onset of pyrolysis of the insulation material [27].

89 Whilst the previous approach stands out by its simplicity, which is easily achievable in engineering
90 terms, it may be very conservative for some scenarios. A more accurate approach should rely on estimating
91 the rates of pyrolysis from the insulation under specific fire scenarios. By determining the pyrolysis
92 behaviour, the evolution of the hazard (potential contribution to the fire and generation of toxic species)
93 can be quantified [28]. This approach requires a pyrolysis model which is able to accurately predict the
94 thermal behaviour of the insulation. In the last decade, such pyrolysis models have been developed and
95 validated [29–32]. These models tend to require a large number of parameters that are often unknown,
96 necessitating inverse modelling techniques that can introduce significant compensation errors [33] and
97 demand a great deal of expertise. An additional handicap on the use of these tools is that the thermal
98 boundary condition under real fire scenarios is difficult to quantify. Consequently, if pyrolysis rates are to
99 be quantified at an appropriate level for engineering design optimisation, simpler approaches are necessary.

100 **1.3. Research aim**

101 This work aims to assess the applicability of a simplified methodology for quantifying pyrolysis rates
102 and temperature evolution from foil-lined closed-cell charring insulation materials under severe conditions
103 of heat exposure. It focusses on small-scale experiments so as to reduce the uncertainty in the assessment,
104 thus precisely controlling the thermal evolution and mass loss of samples under a heating regime that is
105 close to one-dimensional. Despite the fact that characterising the pyrolysis represents a challenge due to the
106 large number of material properties to be quantified, the presented simplified experimental approach still
107 allows prediction of the hazard while keeping the method simple. The success of this approach will allow
108 estimation of pyrolysis rates from this type of insulation in research-driven large-scale experiments and
109 standard testing. Given that the pyrolysis rate represents the main physical variable determining the heat
110 release contribution and yields of toxic species, the application of this methodology will help to improve
111 current testing practices.

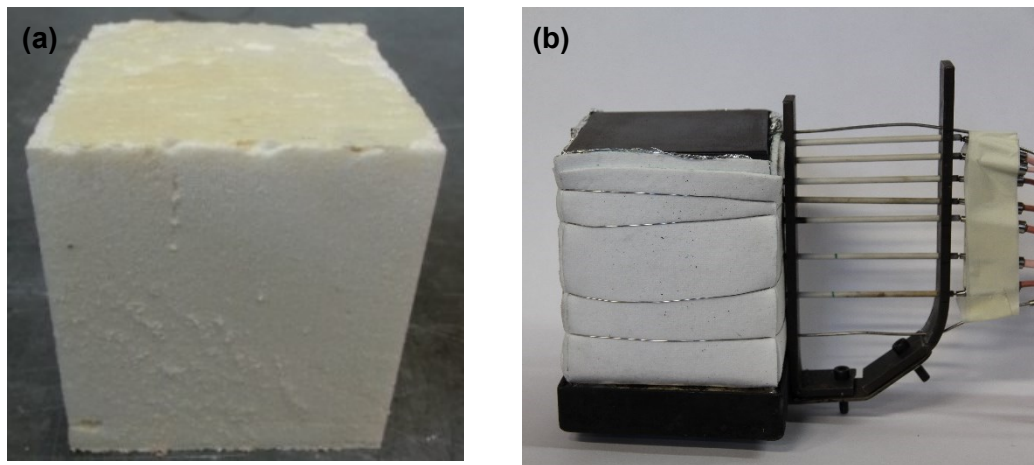
112 **2. Experimental programme description**

113 The experimental programme was designed to explore the applicability of simpler modelling
114 approaches, and based on the use of the Cone Calorimeter apparatus [34] and thermogravimetric
115 experiments. The Cone Calorimeter set-up was modified to remove the pilot spark and to enable heating of
116 the sample by conduction from a metallic plate on the exposed surface. The main measurements consisted
117 of mass loss and temperature within the samples, supported by visual observations. Four experiments were
118 performed for each thermal exposure, two repetitions measuring only mass loss, and two repetitions taking

119 temperature measurements within the samples. The thermogravimetric data corresponded to those
120 presented by the authors elsewhere [35].

121 **2.1. Materials**

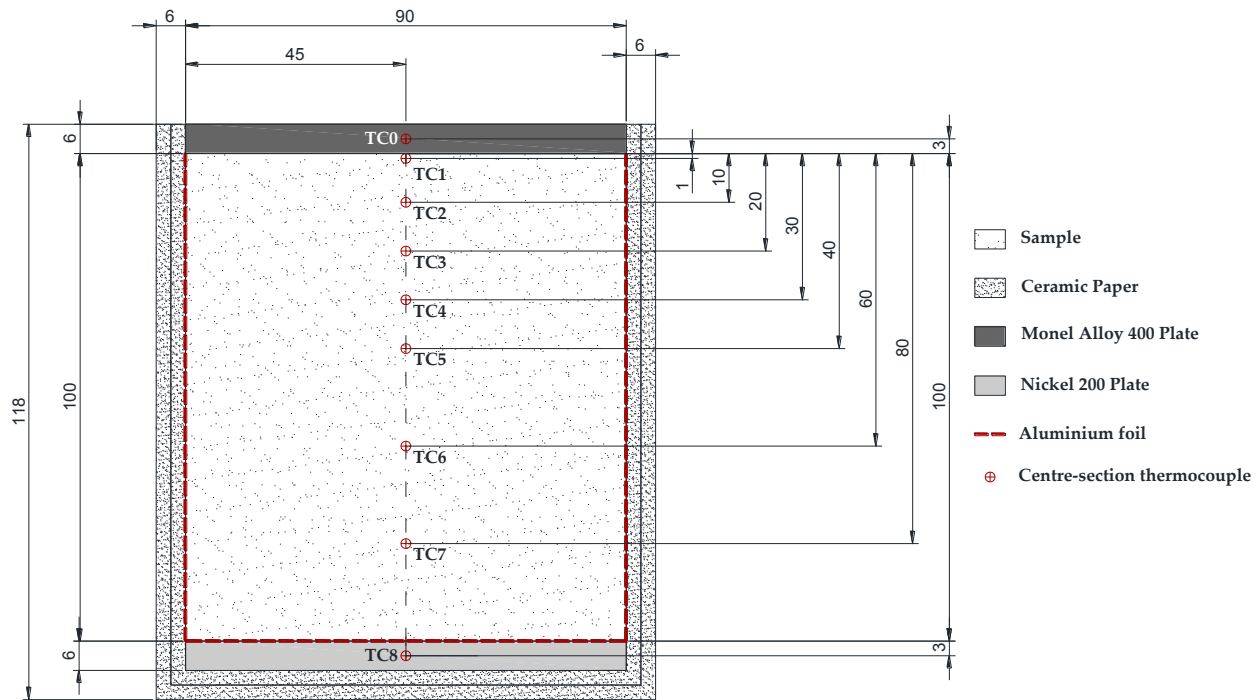
122 The studied insulation material corresponded to a type of rigid polyisocyanurate foam previously
123 described as PIRb elsewhere [20,35]. Samples with a surface area of 90 mm by 90 mm and 100 mm thick
124 were tested for this series of experiments. The metallic plate as boundary element at the surface of the
125 samples corresponded to a 6 mm Monel plate, painted with a high temperature optical black coating of
126 known absorptivity ($\alpha = 0.92$, Medtherm Corporation®). The use of the plate presents a case study
127 representative of a common end-use condition of insulation materials, as these are rarely installed
128 uncovered but behind a lining. The oxidation rate is expected to be reduced or eliminated by using this
129 methodology, therefore also reducing the complexity introduced by the smouldering process for future
130 modelling purposes. A metallic plate (6 mm thick, Nickel 200) was used at the bottom of the sample as a
131 heat sink. A sample with the protective foil layer removed and prepared for testing with the metallic plates
132 on top and bottom is shown in Figure 1a.



133
134 **Figure 1. (a) PIR sample prepared for testing. (b) PIR sample wrapped in aluminium foil and ceramic paper**
135 **with metallic plates and thermocouples inserted into the centre of the sample through ceramic tubes. A**
136 **special holder was designed to keep the thermocouple horizontal during the insertion.**

137 **2.2. Experimental set-up**

138 The samples were wrapped with aluminium foil on the bottom and lateral sides, with the 6 mm Monel
139 plate placed on the top and the 6mm Nickel 200 block at the bottom. Sample and plates were wrapped in
140 two 3 mm thick layers of ceramic insulation paper. The purpose of the aluminium foil was to prevent air
141 penetration into the sample from the sides, as the ceramic paper is a porous element, to promote one
142 dimensional pyrolysis. The real set-up and a schematic drawing of this are shown in Figure 1b and Figure
143 2.



144

145

Figure 2. Schematics of sample preparation.

146

In order to provide a well-characterised experimental set-up to allow modelling to be undertaken, the characterisation of the boundary condition at the back face of the material was achieved by using the 6 mm Nickel 200 plate at the bottom of the samples. This approach was described by *Carvel et al.* [36], who recommended the use of a heat sink for material characterisation purposes. Using a metallic plate on top would act as a dummy surface temperature sensor, although contact resistance effects may induce a thermal gradient between sample and metallic plate. This is discussed in subsequent sections.

152

Several levels of irradiation from the radiant heater were used (25, 45 and 65 kW·m⁻²). The heat fluxes were selected such that different rates of pyrolysis would be achieved. Measurements of temperature were taken within the sample by using 1 mm bead N-type thermocouples. The temperature of the metallic plates on the top and bottom was also measured, but with 1.5 mm bead K-type thermocouples. Thermocouples were installed at various depths at the centre of the section (1, 10, 20, 30, 40, 60, 80 mm) parallel to the exposed surface to reduce the error in the thermocouple reading, which is recommended for materials of particularly low conductivity [37,38]. Ceramic tubes were used to insert the thermocouple into the sample, so as to secure the location of the thermocouple for multiple experiments. Additionally, the exact location of the thermocouples could be visually identified after testing. No temperature correction was considered by the heat losses introduced by the thermocouple. The positioning of the thermocouples is shown in Figure 2. A summary of the conditions for all the performed experiments is presented in Table 1.

162

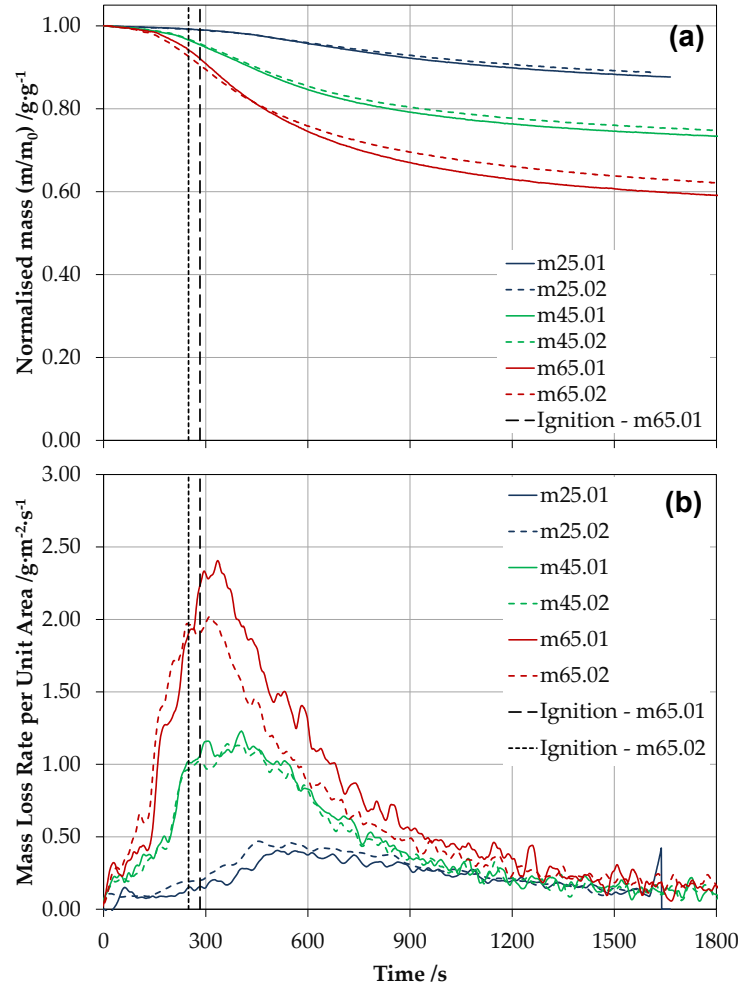
163 **Table 1. Summary of performed experiments**

Material characteristics	Configuration	Incident radiant heat flux range /kW·m ⁻²	Measured parameters
<p style="text-align: center;">PIRb</p> <p>Manufacturer-claimed density: 32 kg·m⁻³</p> <p>Average measured density: 33.0 ± 0.71 kg·m⁻³</p> <p>Estimated thermal inertia: 6.5·10³W²·s·K⁻²·m⁻⁴ [27]</p>	<p>Nominal sample size: 90mm x 90mm x 100mm</p> <p>Top boundary condition: Monel 400 plate (6mm)</p> <p>Wrapping: 2 layers of ceramic paper + 1 layer of aluminium foil</p> <p>Back boundary condition: Nickel 200 plate (6mm) + Ceramic board (25mm)</p> <p>Orientation: Horizontal</p> <p>Pilot: No pilot igniter</p>	<p style="text-align: center;">25, 45, 65</p> <p style="text-align: center;">(4 repetitions)</p>	<p style="text-align: center;">(1) Mass loss (2 repetitions)</p> <p style="text-align: center;">(2) In-depth temperature (2 repetitions)</p>

164 **3. Experimental results and discussion**

165 Figure 3a shows the normalised mass for PIR samples with a Monel plate on top under three constant
 166 levels of irradiation (25, 45 and 65 kW·m⁻²). The normalised mass is obtained by dividing the mass of the
 167 sample at any time by the initial mass (m_0). Vertical dashed lines indicate the time at which the effluent of
 168 pyrolysis gases through the edge of the sample auto-ignited. Results from duplicates show good agreement,
 169 with the major discrepancies observed for the highest heat flux after ignition is observed. This inconsistency
 170 in the results is however expected due to the behaviour of the pyrolysis effluent for each experiment,
 171 resulting in extra heating of the surface metallic plate when ignited. The sample residue obtained after 1800
 172 s of a heat exposure of 25, 45 and 65 kW·m⁻² is approximately 88%, 75% and 60%, respectively.

173 Figure 3b shows the mass loss rate (MLR) per unit area corresponding to the mass loss presented in
 174 Figure 3a. The shape obtained for the three heat fluxes is qualitatively similar, with a MLR peak followed
 175 by a decay, as characteristic of charring materials [39]. The MLR peak increases in magnitude and shifts to
 176 lower times with increasing heat fluxes. Peaks of MLR for 25, 45 and 65 kW·m⁻² are approximately in the
 177 range 0.4-0.5, 1.0-1.2 and 2.0-2.4 g·m⁻²·s⁻¹, respectively. Considering a heat of combustion for the pyrolysis
 178 gases of 13.22 kJ·g⁻¹ as presented by *Hidalgo* [35], the heat release rate per unit area of these peaks
 179 correspond to 6.6, 15.9 and 31.7 kW·m⁻², which are fairly moderate values. Therefore, a significant
 180 contribution to the heat release in a compartment fire from the insulation is only to be expected if a large
 181 surface area is exposed and this is limited to the early stages.



182
183
184

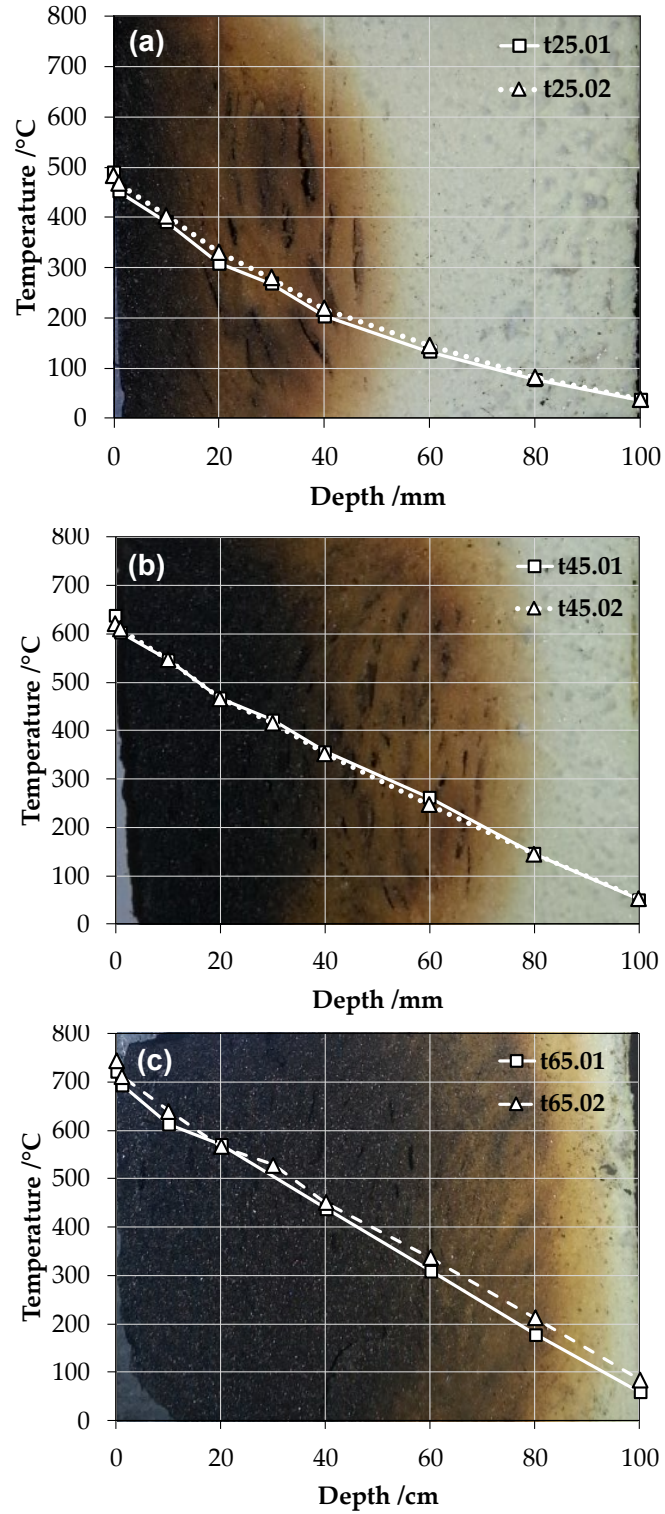
Figure 3. (a) Normalised mass for experiments at 25, 45 and 65 kW·m⁻². Vertical dashed lines indicate the auto-ignition of the pyrolysis effluent. (b) Mass loss rate per unit area.

185
186
187
188
189
190
191

The sample residues for experiments shown in Figure 3 are presented in Figure 4, with a cut through the centre-section. The sample sections show three different regions of discoloration corresponding to the char after pyrolysis (carbonaceous region), reaction zone where pyrolysis process is ongoing (orange region), and virgin material (light yellow/grey region). The regions of discoloration are fairly uniform along the width of the sample, indicating a heating regime similar to 1D. This uniformity is less clear in Figure 4a, corresponding to the sample tested at 25 kW·m⁻². These residues are coupled with the temperature profile during the quasi-steady³ state after 1800 s, obtained from experiments using thermocouples. It should be

³ The term “quasi-steady state” used throughout this paper refers to the stage in which the rate of temperature increase within some sections of the sample is sufficiently low that the net heat flux at the sample surface has achieved an asymptotic behaviour, close to a constant heat flux that defines a steady conduction.

192 noted that the temperature measurements are presented as the original locations in the sample before testing.
193 The samples tested at 25, 45 and 65 kW·m⁻² presented a shrinkage after 1800 s of about 0, 5 and 10 mm,
194 respectively. For ease in the visualisation, the image of the residue has been adapted to the original sample
195 size of 100 mm to fit into the same scale of the temperature-depth diagrams.



196
197
198

Figure 4. PIR residue after 1800 s of heat exposure of (a) 25, (b) 45 and (c) 65 kW·m⁻². The maximum temperature achieved for each depth is presented on top of each cut presented as background.

199 Figure 5 shows the temperature measurements obtained for experiments with thermocouples under 25,
200 45 and 65 kW·m⁻². Duplicated experiments are shown as dashed lines. In general, good repeatability is
201 obtained for experiments at 25 and 45 kW·m⁻², while for 65 kW·m⁻² this is not that good for thermocouples
202 in the 10 mm and 20 mm in-depth position during the transient state, and also for the top plate. The
203 temperature at the top plate experiences a sudden increase due to the auto-ignition of the pyrolysis effluent.
204 Then, the temperature decreases significantly, with a noisy reading, thus indicating a bad contact between
205 thermocouple and plate, which was later corrected.

206 The readings presented in Figure 5 indicate a clear effect of the contact resistance during the
207 experiments. During the transient state the temperature difference between plate and first position within
208 the sample (1 mm) is clearly noticeable with a difference of up to 200 °C. However, once the quasi-steady
209 state is reached, the difference drops to only 20 °C. This is a reasonable result, as the net heat flux through
210 the surface of the sample is large during the transient state, reducing continuously until the quasi-steady
211 state is reached. Given a constant thermal resistance of the contact, a larger heat flux will result in larger
212 temperature gradients. While these considerations about the contact resistance are important for heat
213 transfer modelling, for the present analysis they have few implications as a reading near the surface is also
214 available.

215 Additionally, the obtained measurements indicate that the smouldering process has been successfully
216 mitigated by using the metallic plate and aluminium foil, as the temperature evolution follows the trend of
217 an apparently inert solid under a constant irradiation level and heat losses. The critical temperature proposed
218 by *Hidalgo et al.* [27] for this material (PIR) is 300 °C, which fundamentally represents the onset of hazard
219 (pyrolysis) and corresponds to the primary failure criterion to be considered for the fire safe design of
220 assemblies including insulation. This value is plotted as a horizontal line, showing that samples exposed to
221 25, 45 and 65 kW·m⁻² achieve the critical temperature at the 1 mm in-depth thermocouple at about 520, 285
222 and 220 s, respectively. These times slightly correspond to the period prior to the maximum increase in
223 MLR before the peak, thus validating the conservative definition of critical temperature for charring
224 materials proposed by *Hidalgo et al.* [27].

225 Figure 6 (solid lines) shows the propagation of the front at 300 °C (assumed to correspond to the
226 pyrolysis front) obtained for the three cases presented in Figure 5 by interpolating the temperature profile
227 for each position. Due to the imprecise positioning of some thermocouples and/or density of temperature
228 measurements within the insulation core, it is observed that the position versus time presents a change of
229 curvature, which otherwise would not be expected e.g. at 500 s, 20 mm depth during the 45 kW·m⁻² heat
230 exposure. Complementary to this, the first derivative of this function that represents the spread rate of the
231 front at 300°C is plotted as a dashed line. A maximum spread rate of 2, 5 and 6 mm·min⁻¹ is observed for

232 25, 45 and 65 kW·m⁻², respectively. Consistent with the data of normalised mass, the spread of the pyrolysis
233 front experiences an attenuation/decay due to the charring nature of the foam, which is fundamentally a
234 consequence of a reducing net heat flux at the pyrolysis front. The fact that the char layer is protected by
235 the metallic plate, and therefore not consumed by oxidation, allows the net heat flux at the pyrolysis front
236 to keep decreasing as this progresses in-depth.

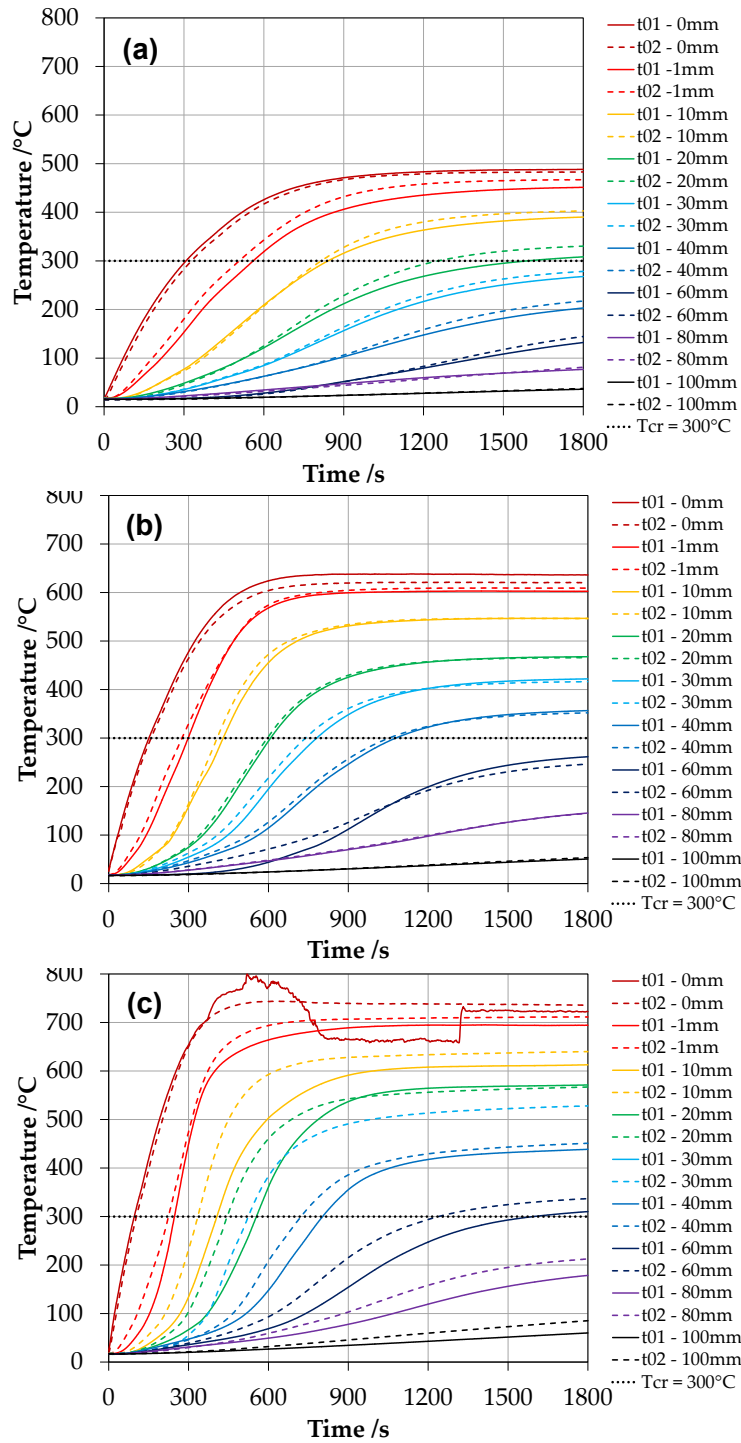
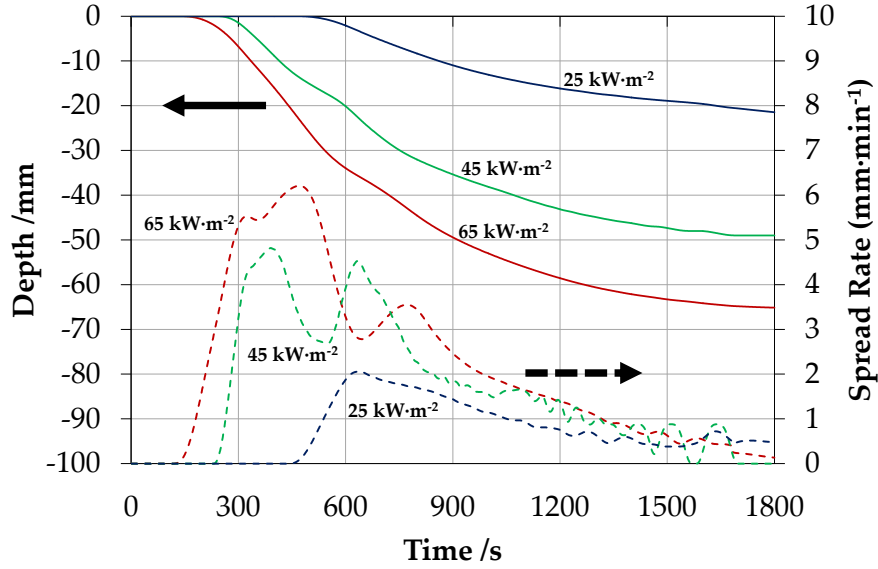


Figure 5. Temperature profiles for a heat exposure of (a) 25, (b) 45 and (c) 65 W·m⁻². Repetition shown as dashed lines.

237
 238
 239
 240



241

242

243

Figure 6. Position of the front at 300 °C (solid lines) and spread rate of this front (dashed lines) for experiments at 25, 45 and 65 kW·m⁻². Interpolated values computed based on data presented in Figure 5.

244

4. Modelling analysis

245

4.1. Principles for the simplified pyrolysis rate assessment

246

247

248

249

250

251

252

253

254

255

256

257

The simplified pyrolysis model is based on the approach already proposed by *Hidalgo et al.* [40]. This approach consists of a two-step decoupled analysis, first solving the heat transfer problem and then followed by the estimation of remaining mass and pyrolysis rates. Despite the fact that effective thermal properties could be obtained to characterise the PIR thermal evolution, in this work modifications are made and the first step is bypassed experimentally without having to solve the diffusion heat transfer within the solid-phase. The approach then consists in determining the mass loss as a function of the thermal evolution. The sample is considered as the space domain $x = L$ (m) divided into N finite differences of thickness Δx_i (m), with i each of the finite differences. As for the analysis in the previous section, the temperature evolution for each finite difference is obtained by linear interpolation. Given that the method is also discretised in time, each time step is defined as j and considered as Δt (s). Then, the normalised sample mass for the time step j is obtained as the following expression representing an integration over the space domain:

$$\bar{m}^j = \frac{\sum_{i=1}^N (\bar{m}_i^j \cdot \Delta x_i)}{L} \quad (1)$$

258

259

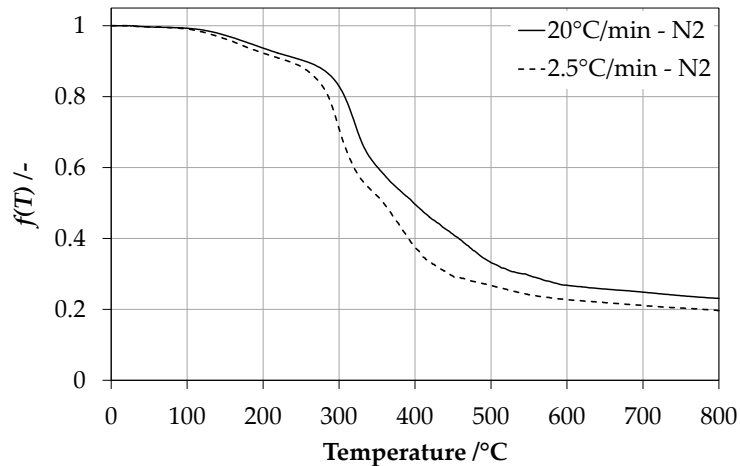
where \bar{m}_i^j is the normalised mass of the finite difference i , which is approximated directly as a function of the temperature $f(T)$:

$$\bar{m}_i^j = f(T) \quad (2)$$

260 The function $f(T)$ establishes the fraction of remaining mass as a function of the temperature in that
 261 finite difference, varying from 0 to 1. To simplify this function and remove uncertainty associated with
 262 fitting of Arrhenius parameters, which depend on the temperature and the concentration/diffusion of oxygen
 263 [41,42], $f(T)$ is defined by direct reference to TGA results under sufficiently low heating rates. The TGA
 264 curves presented in Figure 7 correspond to PIR from the same manufacturer obtained in a non-oxidative
 265 atmosphere and heating rates of 2.5 and 20 °C·min⁻¹ [4]. The normalised mass loss rate can be obtained by
 266 deriving the mass loss over time, which in a discretised form corresponds to the increment of the normalised
 267 mass between time steps divided by the time step. The mass loss rate per unit area can then be calculated
 268 by considering the density of the virgin material ρ_0 (kg·m⁻³) and the thickness of the sample L (m):

$$\dot{m}_p''^j = \rho_0 \cdot L \cdot \frac{\bar{m}^{j-1} - \bar{m}^j}{\Delta t} \quad (3)$$

269 where $\dot{m}_p''^j$ is the mass loss rate per unit area (kg·m⁻²·s⁻¹), or equivalently the rate of pyrolysis per unit area
 270 because no oxidation is considered.



271
 272 **Figure 7. Normalised mass of PIR from the same manufacturer obtained by thermogravimetry under a**
 273 **nitrogen atmosphere at 2.5 and 20°C·min⁻¹ [4].**

274 **4.2. Results**

275 Figure 8 shows the experimental and modelled normalised mass loss rate considering the temperature
 276 profiles presented in Figure 5. Normalised values of mass loss rate are compared so that the error due to
 277 inaccuracy in the dimensions, and therefore density calculation for the modelled MLR, can be minimised.
 278 The experimental normalised MLR is obtained by differentiating the normalised mass curves with respect
 279 to time (as shown in Figure 3a), while the modelled MLR is obtained by integrating the $f(T)$ function for

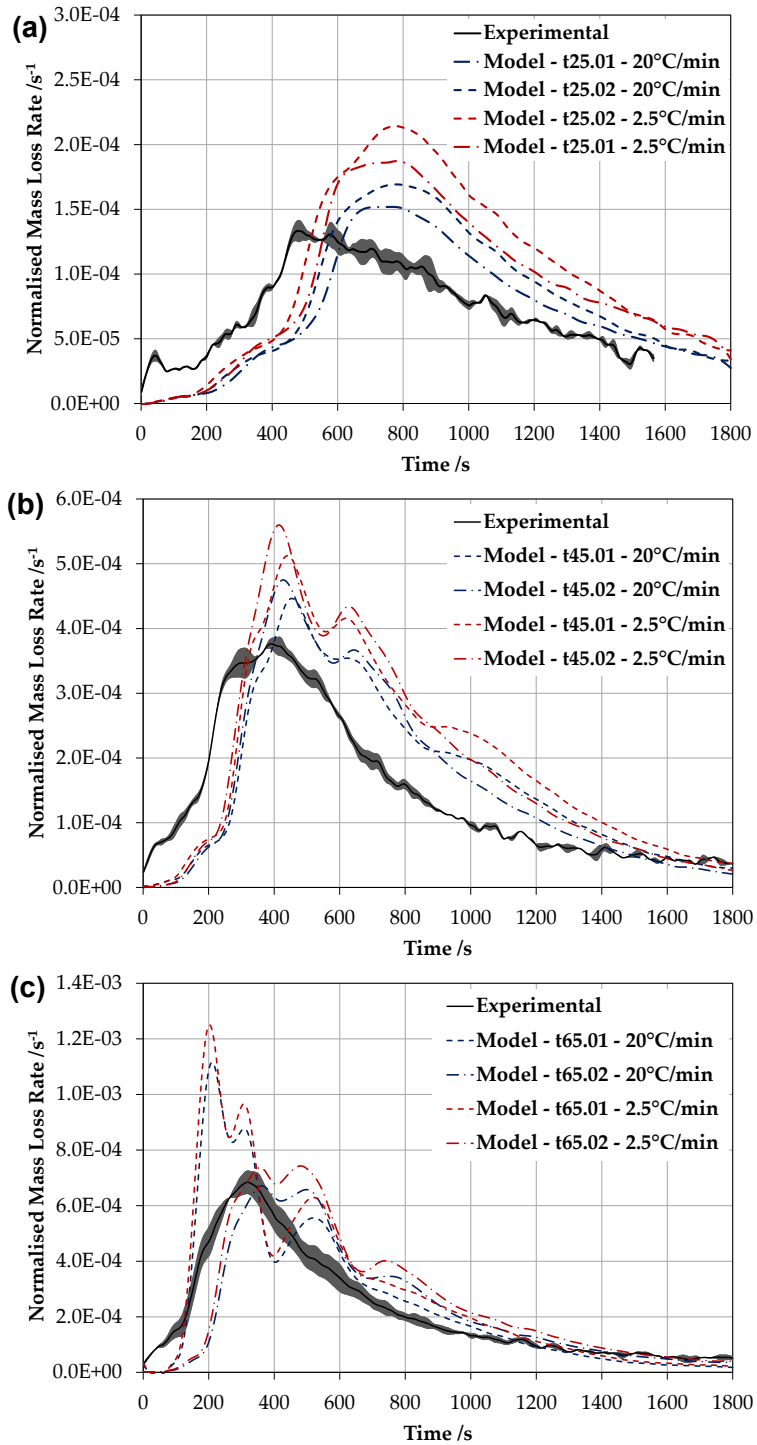
280 the whole thickness for each time step as shown in Eq. 1 and 2, and then differentiating with respect to
281 time.

282 It is observed that the model does not produce a perfect fit with the experimental data. This is however
283 not surprising due to the deliberate simplicity of the proposed approach. Nevertheless, it is clear that the
284 primary mechanisms that characterise the pyrolysis from PIR under different heating scenarios are fairly
285 represented, since the results follow similar trends. The most obvious inaccuracy presented by the model is
286 the delay between experimental and model results. This could be partially attributed to a bad adjustment of
287 the time lines for experiments with and without thermocouples. Other factors that could contribute to this
288 delay are an insufficiently high density of thermocouples near the surface of the material and/or the linear
289 interpolation method. The transport time of the pyrolysis gases could also be a factor, although the time
290 scale is expected to be much lower, of the order of seconds. In any case this is a drawback that can be easily
291 corrected and/or calibrated without affecting the outcomes of the assessment.

292 Another clear conclusion from the results presented in Figure 8 is that the TGA curve for which the
293 model better predicts the experimental results is the one with the highest heating rate used, i.e. $20\text{ }^{\circ}\text{C}\cdot\text{min}^{-1}$
294 ¹. Figure 9 shows the heating rate experienced for various locations (1 and 4 mm) at 25 and 65 $\text{kW}\cdot\text{m}^{-2}$. The
295 derived maximum heating rate is around $140\text{ }^{\circ}\text{C}\cdot\text{min}^{-1}$, while for other regions and heat fluxes the heating
296 rate does not go over $60\text{ }^{\circ}\text{C}\cdot\text{min}^{-1}$. The slight overestimation of the modelled MLR is consistent with these
297 results, as $20\text{ }^{\circ}\text{C}\cdot\text{min}^{-1}$ is not as high as the heating experienced at certain locations. However, the observed
298 heating is obviously not constant, with expected average values closer to the $20\text{ }^{\circ}\text{C}\cdot\text{min}^{-1}$ threshold. Despite
299 the fact that using this heating rate as input for the function $f(T)$ may lead to a slight overestimation of
300 results, in engineering practice this could still be a conservative and practical approach. As a matter of fact,
301 the results using a lower heating rate do not show significantly large overestimations.

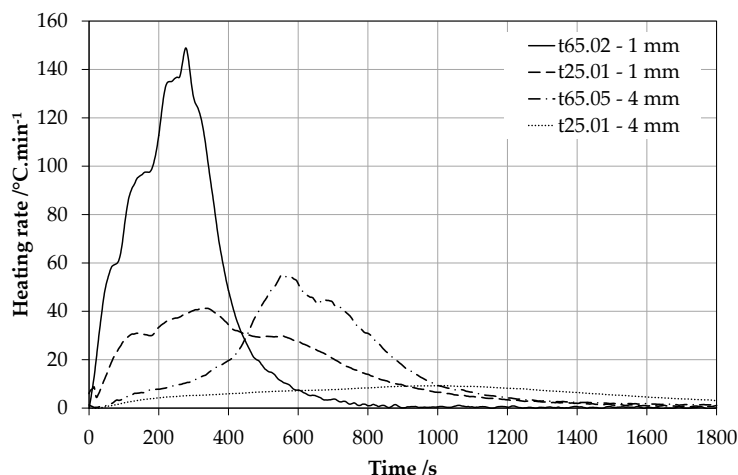
302 Figure 8c shows that the model based on the data from one of the repetitions with thermocouples at 65
303 $\text{kW}\cdot\text{m}^{-2}$ presents a clear and more significant overestimation of the MLR. This is probably mainly due to
304 inaccurate positioning of the thermocouples for this particular experiment, which did not use a stiffening
305 system as presented in Figure 1b. This highlights the importance of the position and density of temperature
306 measurements in practice.

307



308
 309
 310
 311

Figure 8. Experimental and modelling results for (a) 25, (b) 45, and (c) 65 $kW\cdot m^{-2}$. Experimental curve corresponds to the average between two repetitions, and the shading is the maximum deviation from repetitions to the average.



312

313 **Figure 9. First derivative of temperature measurements at 1 and 4 mm at 25 and 65 kW·m⁻².**

314 **4.3. Limitations and model uncertainties**

315 **Oxidative conditions**

316 The proposed model is based on the assumption that no smouldering occurs. Therefore, the applicability
 317 of this approach is only valid for non-permeable materials that do not allow oxygen transfer through the
 318 matrix, thus the thermal decomposition corresponds to non-oxidative conditions as presented in Figure 7.
 319 If oxidative conditions are produced on the top, exposed surface, the calculated rate of pyrolysis is expected
 320 to still be reasonably reproduced, however the total mass loss rate would be under-predicted as the char
 321 oxidation would be neglected.

322 The shrinking behaviour of the material would lead to the creation of a gap between lining and
 323 insulation. Once this is achieved, air flow may be expected within the gap. After this has occurred the
 324 smouldering process may become a relevant hazardous event that would increase the heat flow through the
 325 insulation reaction zone.

326 **Heating rate**

327 While it is normally admitted that the heating experienced by burning fuels is much larger than heating
 328 rates obtained by thermogravimetry [43], this is clearly not the case for charring materials such as PIR. The
 329 effectiveness of the approach then resides in the low and reducing heating rates experienced by the reaction
 330 and virgin zones, as shown in Figure 9. The results presented in the previous section indicate that a heating
 331 rate of 20 °C·min⁻¹ provides a reasonable accuracy for all the heating scenarios studied and the particular
 332 thickness of 100 mm. The trend in Figure 8 indicates that increased heating rates could provide better
 333 results, since 20 °C·min⁻¹ is a heating rate lower than those observed in Figure 9 during the peaks of MLR;
 334 however the improvement appears to be not very substantial.

335 **Thermal interpolation**

336 As shown in Figure 8c, an accurate position of the thermocouples and their spacing is essential to
337 obtaining sensible results. For the present case of 100 mm thick samples, 10 mm spacing for regions near
338 the surface and 20 mm for regions far from the surface are able to provide sufficiently good results. While
339 smaller spacing may result in greater accuracy, a system to secure the thermocouple as presented in this
340 experimental programme seems essential, as the error in spacing can easily be of order ± 3 mm when
341 thermocouples are inserted without a stiffening system, due to the friable nature of the foam. In addition,
342 the thermal mass of an increased number of thermocouples may result in a 'heat sink' effect, leading to
343 premature quenching of the reaction.

344 The interpolation method used to obtain thermal evolution between thermocouple measurements was
345 linear. The accuracy of this approach is proportional to the density of thermocouples. Despite the simplicity
346 of the approach, it seems to provide accurate results.

347 **Heat transfer dimensionality**

348 The accuracy of the results from this experimental programme also depend on the one-dimensionality
349 of the heat transfer. Observations of the colour change of the experimental sample residues qualitatively
350 indicates that the 1D assumption seems to be fairly correct. While this could be an issue for the presented
351 experimental programme, since the wrapping material had higher conductivity than the samples, in real
352 scenarios however this assumption is rather controlled by the uniformity of the heating boundary condition.
353 For that case, the accuracy would then be limited by the density of measuring points over the surface area
354 of the building assembly being studied.

355

356 **5. Applicability for fire safety engineering**

357 Since the primary fire hazard from these types of insulation can be associated to the pyrolysis process,
358 the main parameter to be quantified is the rate of pyrolysis gas release. Despite the fact that there is large
359 uncertainty with regard to the location, conditions and instant at which these will ignite, due to, for instance,
360 the ventilation conditions of the construction system, the conservative approach is to assume that these
361 would instantaneously contribute to the fire. This way the risk can be quantified more easily.

362 The presented method, although not extremely accurate, presents a reasonable level of precision for
363 engineering purposes where the degree of uncertainty in other parameters is already high. Two clear
364 applications can be found for the present model as: (1) pyrolysis estimation for fire testing such as large-
365 scale experiments or standard testing, and (2) for quantitative design purposes.

366 **5.1. Model testing**

367 The presented simplified method can be used to develop a model of the pyrolysis behaviour under well-
368 defined testing conditions. The concept consists of running ad-hoc and/or standard fire testing including a
369 series of thermocouples to allow an *a posteriori* quantification of the pyrolysis behaviour from the
370 insulation. This approach would also allow quantification of the effectiveness of various protection systems,
371 to allow an optimised design solution to be generated. The provision of pyrolysis predictions can
372 complement heat release rate calculations and measurements of gas species from the generated smoke.
373 Within this scope, error bars need to be acknowledged, based on the model limitations and testing conditions
374 noted previously. Clearly, if consistent data are used, expected errors can be quantified and delimited. The
375 potential of this approach resides in the low-cost solution for improved product development, thus reducing
376 costly research based on full-scale testing.

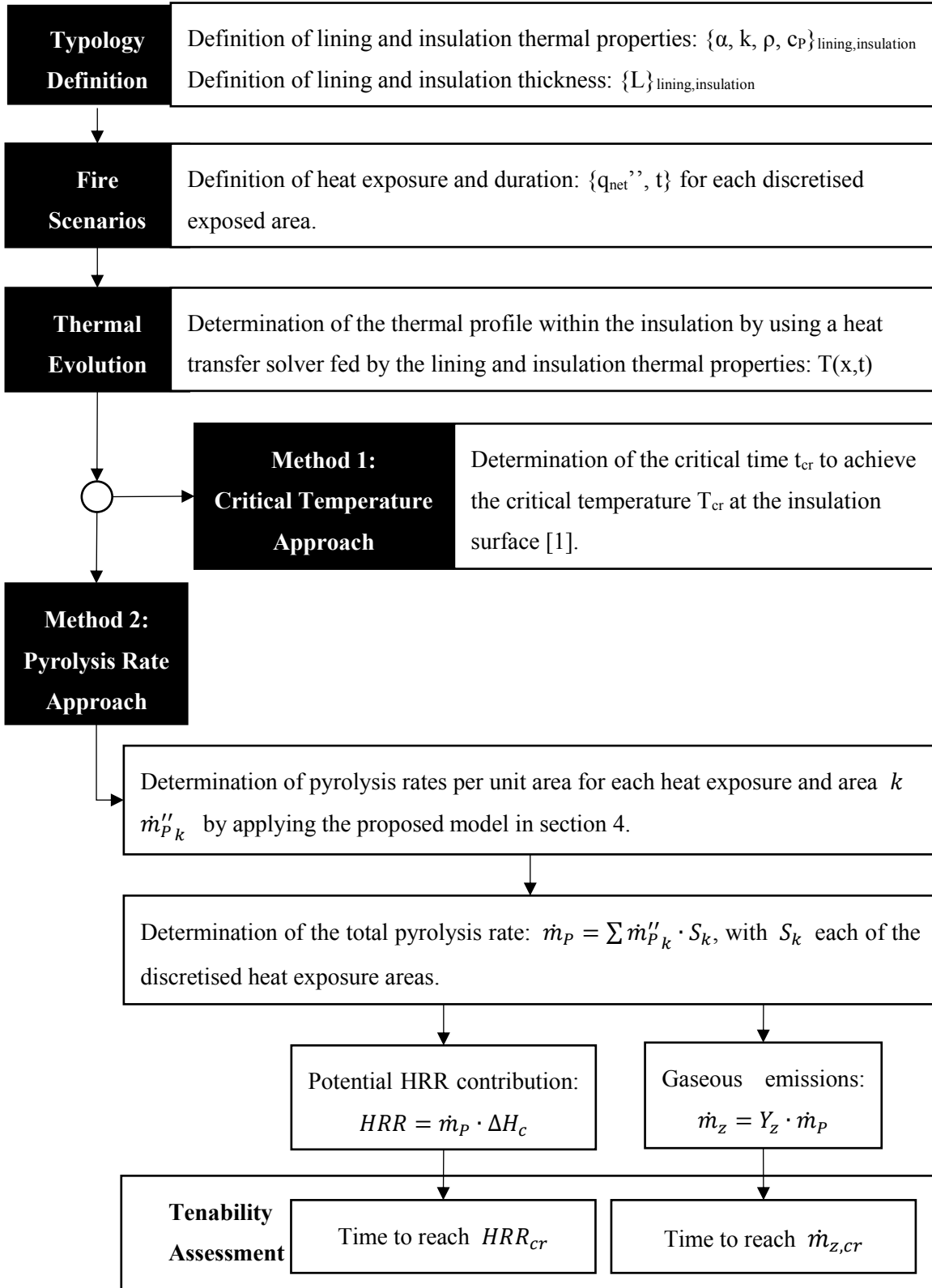
377 **5.2. Hazard quantification**

378 The proposed methodology can lead to evaluation of designs, by which the fire hazard from insulation
379 materials can be quantified explicitly if a series of assumptions and hypotheses are established. A diagram
380 describing the application of the methodology for design purposes is presented in Figure 10. The approach
381 consists of evaluating the time to achieve a potential hazardous heat release contribution and gaseous
382 emissions from the insulation.

383 The first step is based on the definition of effective thermal properties and initial thickness for lining
384 and insulation. Then, a series of fire scenarios defined as the conditions of heat exposure (thermal boundary
385 conditions), their respective area of exposure, and exposure time have to be proposed. Next, the thermal
386 evolution of the system lining-insulation has to be estimated for each boundary condition by using a heat
387 transfer solver. For simplicity, the problem can be simplified as a one-dimensional problem and a perfect
388 contact can be assumed between insulation and lining, which are conservative assumptions. At this stage
389 practitioners can either apply the simplified methodology based on a critical temperature proposed
390 elsewhere [26], or alternatively apply the uncoupled pyrolysis model presented in previous sections in order
391 to estimate the pyrolysis rate for each area of exposure. If the former is applied, the failure time of the
392 insulation system is defined as the time when the insulation reaches the critical temperature at the surface.
393 If the latter is applied, a total rate of pyrolysis gas generation needs to be calculated as the sum from each
394 of the exposure areas. The potential heat release contribution can be obtained by multiplying the generation
395 rate by the corresponding effective heat of combustion, while analogously the potential gaseous emissions
396 can be obtained by multiplying by the corresponding yields. The failure time then can be defined as the
397 time to reach a critical value of HRR or emission concentration.

398 While the calculation of gaseous emissions represents an ambitious task, as these strongly depend on
399 conditions such as oxygen concentration and temperature [44], a series of hypotheses can be set if further
400 toxicity assessments are pursued. For instance, these values can be used as inputs for CFD modelling in
401 order to estimate fractional effective concentrations/doses for tenability assessments [45]. Similarly,
402 potential HRR contributions can be used for tenability assessments in fire (zone/CFD) models.

403 The potential of this approach resides in the fact that the data required to develop these quantifications
404 can be obtained by using bench-scale tests (for instance, thermogravimetric data or material properties such
405 as thermal properties, yields or heat of combustion) that are often readily available from manufacturers, or
406 by using values presented in the literature.



407
408
409

Figure 10. Evaluation process to determine the time to reach unsafe conditions for a specific wall typology and fire scenario (boundary condition).

410

411 **6. Conclusions and future work**

412 This paper has presented the application of a simplified methodology to estimate pyrolysis rates from
413 charring insulation materials such as rigid polyisocyanurate foam based on experimental temperature
414 measurements. In order to verify the proposed method, an experimental programme consisting of 100 mm
415 thick samples of rigid polyisocyanurate foam was conducted using a Cone Calorimeter, obtaining
416 measurements of mass loss and temperature within the core of the material. A Monel plate was used on top
417 of the sample in order to represent a simpler boundary condition by eliminating the smouldering process of
418 the charred material.

419 The proposed approach, although not showing a perfect fit with experimental data, has been proved to
420 provide a reasonably good prediction of the pyrolysis rate from a rigid closed-cell polyisocyanurate foam
421 under different scenarios of heat exposure using constant levels of irradiation (25, 45 and 65 kW·m⁻²), and
422 a sample thickness of 100 mm. The simplified methodology is based on the direct use of TGA data to obtain
423 mass loss measurements relying on temperature readings. Since this methodology is limited to non-
424 oxidative conditions, the method must be applied for configurations where the insulation is covered by a
425 lining or barrier. The use of TGA data with a heating rate of 20 °C·min⁻¹ and under a non-oxidative
426 atmosphere has been shown to provide a good accuracy, with a slight overestimation in the modelled
427 normalised mass loss rate. The position and density of temperature measurements has been highlighted to
428 be one of the most important factors for achieving accurate results.

429 The presented method presents a reasonable level of precision for engineering purposes where the degree
430 of uncertainty in other parameters is already high. This approach presents potential for fire safety
431 engineering applications in two domains: (1) as a complementary technique to improve the interpretation
432 of results from standard and ad-hoc testing, and (2) as a design technique for the evaluation of potential
433 heat release contribution and gaseous emissions of assemblies incorporating insulation materials. The
434 former approach can be used to allow a better characterisation of the fire performance of the insulation,
435 without the necessity of developing complex numerical models. The latter approach can be used to evaluate
436 designs by which the fire hazard from insulation materials can be quantified explicitly.

437 Since the approach presented in this paper is limited to experimental measurements of temperature, it
438 may be insufficient for general design purposes, as it is scenario dependent. The main potential of the
439 proposed methodology is that it would allow faster and more effective product development, thus reducing
440 costly research based on full-scale testing. Therefore, future work should focus on determining effective
441 thermal properties that could reproduce the thermal behaviour of the material and treat the problem as a

442 two-step uncoupled analysis, as shown elsewhere [40]. The experimental work presented within this paper
443 can further be used for the determination of these effective model parameters.

444 **Acknowledgements**

445 The authors would like to gratefully acknowledge funding from Rockwool International A/S towards
446 the Ph.D. studies of Juan P. Hidalgo. Michal Krajcovic and Qing Ye are gratefully acknowledged for their
447 precious lab assistance on the performed experimental programme.

448 **References**

- 449 [1] Directive 2010/31/EU of the European Parliament and of the Council of 19 May 2010 on the
450 energy performance of buildings (recast), 2010. doi:doi:10.3000/17252555.L_2010.153.eng.
- 451 [2] C. Despret, M. Economidoe, N. Griffiths, J. Maio, I. Nolte, O. Rapf, eds., Principles for
452 nearly zero-energy buildings, paving the way for effective implementation of policy
453 requirements, Buildings Performance Institute Europe, 2011.
454 http://bpie.eu/documents/BPIE/publications/LR_nZEB_study.pdf.
- 455 [3] A.M. Papadopoulos, State of the art in thermal insulation materials and aims for future
456 developments, *Energy Build.* 37 (2005) 77–86. doi:10.1016/j.enbuild.2004.05.006.
- 457 [4] J.P. Hidalgo-Medina, Performance-based methodology for the fire safe design of insulation
458 materials in energy efficient buildings, University of Edinburgh, 2015.
459 <http://hdl.handle.net/1842/10601>.
- 460 [5] A. Witkowski, A.A. Stec, R.T. Hull, Thermal Decomposition of Polymeric Materials, in:
461 SFPE Handb. Fire Prot. Eng., 5th ed., Springer, 2016: pp. 167–254. doi:10.1007/978-1-4939-
462 2565-0.
- 463 [6] C. Dick, E. Dominguez-Rosado, B. Eling, J.J. Liggat, C.I. Lindsay, S.C. Martin, M.H.
464 Mohammed, G. Seeley, C. Snape, The flammability of urethane-modified
465 polyisocyanurates and its relationship to thermal degradation chemistry, *Polymer*
466 (Guildf). 42 (2001) 913–923. doi:10.1016/S0032-3861(00)00470-5.
- 467 [7] E. Dominguez-Rosado, J.J. Liggat, C.E. Snape, B. Eling, J. Pichtel, Thermal degradation of
468 urethane modified polyisocyanurate foams based on aliphatic and aromatic polyester
469 polyol, *Polym. Degrad. Stab.* 78 (2002) 1–5. doi:10.1016/S0141-3910(02)00086-1.
- 470 [8] I. Vitkauskienė, R. Makuška, U. Stirna, U. Cabulis, Thermal properties of polyurethane-
471 polyisocyanurate foams based on poly(ethylene terephthalate) waste, *Medziagotyra.* 17
472 (2011) 249–253. doi:10.5755/j01.ms.17.3.588.
- 473 [9] N. Cinausero, B. Howell, G. Schmaucks, G. Marosi, Z. Brzozowski, J.-M.L. Cuesta, G.
474 Nelson, G. Camino, C. Wilkie, A. Fina, J. Hao, S. Nazare, E. Kandore, J. Staggs, Y.C. Wang,
475 S. Duquesne, R. Hicklin, P. Wakelyn, S. Gaan, A.R. Horrocks, P. Joseph, D. Purser, A. Stec,
476 M. Hassan, C. Kindness, B.B. Marosfoi, T.R. Hull, B.K. Kandola, Fire retardancy of

- 477 polymers: new strategies and mechanisms, The Royal Society of Chemistry, 2009.
478 doi:10.1039/9781847559210.
- 479 [10] K.T. Paul, Burning characteristics of materials, *Fire Mater.* 3 (1979) 223–231.
480 doi:10.1002/fam.810030408.
- 481 [11] K.T. Paul, Characterization of the burning behaviour of polymeric materials, *Fire Mater.* 8
482 (1984) 137–147. doi:10.1002/fam.810080304.
- 483 [12] J.M. Buist, S.J. Grayson, W.D. Woolley, eds., *Fire and Cellular Polymers*, Springer
484 Netherlands, 1986. doi:10.1007/978-94-009-3443-6.
- 485 [13] M.J. Scudamore, P.J. Briggs, F.H. Prager, Cone calorimetry—a review of tests carried out
486 on plastics for the association of plastic manufacturers in Europe, *Fire Mater.* 15 (1991) 65–
487 84. doi:10.1002/fam.810150205.
- 488 [14] J.G.Q. Thomas G. Cleary, Flammability characterization of foam plastics (NISTIR 4664),
489 1991.
- 490 [15] M. Modesti, A. Lorenzetti, F. Simioni, M. Checchin, Influence of different flame retardants
491 on fire behaviour of modified PIR/PUR polymers, *Polym. Degrad. Stab.* 74 (2001) 475–479.
492 doi:10.1016/S0141-3910(01)00171-9.
- 493 [16] A. Tewarson, R.F. Pion, Flammability of plastics-I. burning intensity, *Combust. Flame.* 26
494 (1976) 85–103. doi:10.1016/0010-2180(76)90059-6.
- 495 [17] M. Modesti, A. Lorenzetti, Improvement on fire behaviour of water blown PIR-PUR foams:
496 use of an halogen-free flame retardant, *Eur. Polym. J.* 39 (2003) 263–268. doi:10.1016/S0014-
497 3057(02)00198-2.
- 498 [18] A.P. Mouritz, A.G. Gibson, *Fire properties of polymer composite materials*, Springer, 2006.
499 doi:10.1007/978-1-4020-5356-6.
- 500 [19] M.L. Auad, L. Zhao, H. Shen, S.R. Nutt, U. Sorathia, Flammability properties and
501 mechanical performance of epoxy modified phenolic foams, *J. Appl. Polym. Sci.* 104 (2007)
502 1399–1407. doi:10.1002/app.24405.
- 503 [20] J.P. Hidalgo, J.L. Torero, S. Welch, Fire performance of plasterboard-insulation assemblies
504 consisting of closed-cell charring insulation materials, in: *Conf. Proc. Fourteenth Int.*
505 *Interflam Conf.*, 2016: pp. 1507–1518.
- 506 [21] D.D. Drysdale, Fundamentals of the fire behaviour of cellular polymers, in: J.M. Buist, S.J.
507 Grayson, W.D. Woolley (Eds.), *Fire Cell. Polym.*, Springer Netherlands, Dordrecht, 1986:
508 pp. 61–75. doi:10.1007/978-94-009-3443-6_4.
- 509 [22] B. Meacham, B. Poole, J. Echeverria, R. Cheng, *Fire safety challenges of green buildings*,
510 Springer, 2012. doi:10.1007/978-1-4614-8142-3.
- 511 [23] U. Krause, W. Grosshandler, L. Gritzo, The International FORUM of fire research directors:
512 a position paper on sustainability and fire safety, *Fire Saf. J.* 49 (2012) 79–81.
513 doi:10.1016/j.firesaf.2012.01.003.

- 514 [24] BS EN 13501-1:2007+A1:2009 Fire classification of construction products and building
515 elements. Classification using test data from reaction to fire tests, 2007.
- 516 [25] BS EN 1363-1:2012 Fire resistance tests. General requirements, 2012.
- 517 [26] J.P. Hidalgo, S. Welch, J.L. Torero, Performance criteria for the fire safe use of thermal
518 insulation in buildings, *Constr. Build. Mater.* 100 (2015) 285–297.
519 doi:10.1016/j.conbuildmat.2015.10.014.
- 520 [27] J.P. Hidalgo, S. Welch, J.L. Torero, Design tool for the definition of thermal barriers for
521 combustible insulation materials, in: *Proc. 2nd IAFSS Eur. Symp. Fire Saf. Sci.*, 2015: pp.
522 166–170.
- 523 [28] D. Drysdale, *An Introduction to Fire Dynamics*, 3rd ed., Wiley, 2011.
- 524 [29] B. Moghtaderi, V. Novozhilov, D. Fletcher, J.H. Kent, An integral model for the pyrolysis
525 of non-charring materials, *Fire Mater.* 21 (1997) 7–16.
- 526 [30] J.E.J. Staggs, Simple model of polymer pyrolysis including transport of volatiles, *Fire Saf.*
527 *J.* 34 (2000) 69–80. doi:10.1016/S0379-7112(99)00043-0.
- 528 [31] C. Lautenberger, C. Fernandez-Pello, Generalized pyrolysis model for combustible solids,
529 *Fire Saf. J.* 44 (2009) 819–839. doi:10.1016/j.firesaf.2009.03.011.
- 530 [32] S.R. Wasan, P. Rauwoens, J. Vierendeels, B. Merci, An enthalpy-based pyrolysis model for
531 charring and non-charring materials in case of fire, *Combust. Flame.* 157 (2010) 715–734.
532 doi:10.1016/j.combustflame.2009.12.007.
- 533 [33] N. Bal, G. Rein, On the effect of inverse modelling and compensation effects in
534 computational pyrolysis for fire scenarios, *Fire Saf. J.* 72 (2015) 68–76.
535 doi:10.1016/j.firesaf.2015.02.012.
- 536 [34] BS 476-15:1993, ISO 5660-1:1993 Fire tests on building materials and structures. Method for
537 measuring the rate of heat release of products, 1993.
- 538 [35] J.P. Hidalgo, J.L. Torero, S. Welch, Experimental characterisation of the fire behaviour of
539 thermal insulation materials for a performance-based design methodology, *Fire Technol.*
540 (in press). doi:10.1007/s10694-016-0625-z.
- 541 [36] R. Carvel, T. Steinhaus, G. Rein, J.L. Torero, Determination of the flammability properties
542 of polymeric materials: a novel method, *Polym. Degrad. Stab.* 96 (2011) 314–319.
543 doi:10.1016/j.polymdegradstab.2010.08.010.
- 544 [37] J. V Beck, Thermocouple temperature disturbances in low conductivity materials, *J. Heat*
545 *Transfer.* 84 (1962) 124–131. doi:10.1115/1.3684310.
- 546 [38] P. Reszka, In-depth temperature profiles in pyrolyzing wood, University of Edinburgh,
547 2008.
- 548 [39] B. Scharrel, T.R. Hull, Development of fire-retarded materials—interpretation of cone
549 calorimeter data, *Fire Mater.* 31 (2007) 327–354. doi:10.1002/fam.949.
- 550 [40] J.P. Hidalgo, P. Pironi, R.M. Hadden, S. Welch, A framework for evaluating the thermal

- 551 behaviour of carbon fibre composite materials, in: Proc. 2nd IAFSS Eur. Symp. Fire Saf.
552 Sci., 2015: pp. 195–200.
- 553 [41] C. Di Blasi, Modeling and simulation of combustion processes of charring and non-
554 charring solid fuels, Prog. Energy Combust. Sci. 19 (1993) 71–104. doi:10.1016/0360-
555 1285(93)90022-7.
- 556 [42] G. Rein, C. Lautenberger, A.C. Fernandez-Pello, J.L. Torero, D.L. Urban, Application of
557 genetic algorithms and thermogravimetry to determine the kinetics of polyurethane foam
558 in smoldering combustion, Combust. Flame. 146 (2006) 95–108.
559 doi:10.1016/j.combustflame.2006.04.013.
- 560 [43] C.L. Beyler, M.M. Hirschler, Thermal decomposition of polymers, in: SFPE Handb. Fire
561 Prot. Eng. 2, 1995: pp. 111–131.
- 562 [44] A.A. Stec, T.R. Hull, Assessment of the fire toxicity of building insulation materials, Energy
563 Build. 43 (2011) 498–506. doi:10.1016/j.enbuild.2010.10.015.
- 564 [45] V. Mozer, M. Smolka, P. Tofilo, Threat level assessment of smoke emissions from
565 compartment boundaries, in: 2nd Eur. Symp. Fire Saf. Sci., 2015: pp. 284–288.
- 566